Chapter 20

Theoretical Stellar Evolution

Arthur N. Cox, Stephen A. Becker, and W. Dean Pesnell

20.1 BASIC EQUATIONS OF STELLAR STRUCTURE

by Stephen A. Becker

20.1.1 List of Symbols

A_a	Atomic mass of particle a
a	Radiation density constant
c	Speed of light in vacuum
d	Distance traveled by overshooting element from the stable convective boundary
G	Gravitational constant
g	Gravitational acceleration
H_P	Pressure scale height
$L(r)$	Energy transferred per second through a sphere of radius r
L_*	Stellar luminosity
$\mathcal{M}(r)$	Mass in a sphere of radius r
$\mathcal{M}_*$	Stellar mass
$\dot{\mathcal{M}}_*$	Stellar mass-loss rate in $\mathcal{M}_\odot$/yr
$\mathcal{M}_\odot$	Solar mass
N_A	Avogadro's number (6.0221×10^{23} mol^{-1})
n_a	Number density of particle a
P	Pressure
Q	Energy generated per nuclear reaction in MeV
R_*	Stellar radius
r	Nuclear reaction rate or radius
S	Entropy per unit mass
T	Temperature
$T_{\rm eff}$	Effective temperature of the star
t	Time
X_a	Mass fraction of particle a
ϵ	Nuclear energy generation ergs per g s
Γ_2	Second adiabatic exponent
κ	Rosseland mean opacity
ρ	Density
τ_a	Mean lifetime of particle a in a nuclear reaction

All units are in cgs units except where stated otherwise.

For an Eulerian one-dimensional (1D) treatment (r, radius as the independent variable), which assumes hydrostatic equilibrium and neglects rotation and magnetic fields, one has for a nonbinary star the following equations.

For conservation of mass,

$$\frac{d\mathcal{M}(r)}{dr} = 4\pi r^2 \rho(r). \tag{20.1}$$

For conservation of thermal energy,

$$\frac{dL(r)}{dr} = 4\pi r^2 \rho(r) \left[\epsilon(r) - T(r)\frac{dS}{dt}\right]. \tag{20.2}$$

For conservation of momentum (hydrostatic equilibrium),

$$\frac{dP(r)}{dr} = -\rho(r)\frac{G\mathcal{M}(r)}{r^2}. \tag{20.3a}$$

In the relativistic limit such as the case for neutron stars, the Oppenheimer–Volkoff equation of hydrostatic equilibrium applies:

$$\frac{dP(r)}{dr} = -\frac{G\left[\rho(r) + P(r)/c^2\right]\left[\mathcal{M}(r) + 4\pi r^3 P(r)/c^2\right]}{r^2\left[1 - 2G\mathcal{M}(r)/rc^2\right]}. \tag{20.3b}$$

For energy transport,

$$\frac{dT(r)}{dr} = -\frac{3}{4ac}\frac{\kappa(r)\rho(r)}{T^3(r)}\frac{L(r)}{4\pi r^2} \quad \text{(radiative equilibrium)}, \tag{20.4a}$$

$$\frac{dT(r)}{dr} = \left(\frac{dT(r)}{dr}\right)_{\text{ad}} = \frac{\Gamma_2 - 1}{\Gamma_2}\frac{T(r)}{P(r)}\frac{dP(r)}{dr} \quad \text{(adiabatic convection)}. \tag{20.4b}$$

Equation (20.4b) is used whenever

$$-\frac{dT(r)}{dr} > -\left(\frac{dT(r)}{dr}\right)_{\text{ad}} \tag{20.5}$$

(see [1–3]).

Where convection is not adiabatic (such as near the stellar surface), a different expression for Equation (20.4b) should be used [2].

These differential equations also require five specific functions of the local thermodynamic state (at r) obtained from the microphysics:

$$\epsilon = \epsilon(\rho, T, \text{composition}), \tag{20.6a}$$

$$P = P(\rho, T, \text{composition}), \tag{20.6b}$$

$$\kappa = \kappa(\rho, T, \text{composition}), \tag{20.6c}$$

$$S = S(\rho, T, \text{composition}), \tag{20.6d}$$

$$\Gamma_2 = \Gamma_2(\rho, T, \text{composition}). \tag{20.6e}$$

Equation (20.6a), the energy generation rate, includes the effect of neutrino generation as a negative contribution. This relation, as well as Equation (20.6b), the equation of state, and (20.6c), the opacity, are discussed in more detail in the following sections. See [1–3] for more on Equations (20.6d) and (20.6e). Time dependence enters both through Equation (20.2) and the fact that the composition changes with time due to nuclear reactions, which generally allows the stellar model to evolve slowly in a quasistatic manner. When the evolution ceases to be quasistatic, Equations (20.3a) and (20.3b) need to be modified to include an acceleration term.

The basic boundary conditions are

$$\begin{aligned} &\mathcal{M}(r) \to 0, \qquad L(r) \to 0 \qquad \text{for} \quad r \to 0 \quad \text{(central conditions)}, \\ &\mathcal{M}(r) \to \mathcal{M}_*, \qquad L(r) \to L_* \qquad \text{for} \quad r \to R_* \quad \text{(surface conditions)}. \end{aligned}$$

In addition, the variables P and T approach their photospheric values, which are estimated from stellar atmosphere theory [1–4].

The alternative Lagrangian treatment of the stellar structure equations (m, mass as the independent variable) can be found in [4].

A good introduction on how the basic equations of stellar structure are modified for nonspherical rotating stars and on stars with magnetic fields can be obtained in [5] and [6].

20.2 STELLAR NUCLEAR ENERGY GENERATION

by Stephen A. Becker

20.2.1 Two-Body Interactions

For $a + b \rightarrow c + d + e$, where e may or may not be present (for example, $^1\mathrm{H} + {}^2\mathrm{H} \rightarrow {}^3\mathrm{He} + \gamma$, or $^{15}\mathrm{N} + {}^1\mathrm{H} \rightarrow {}^{12}\mathrm{C} + {}^4\mathrm{He}$, or $^1\mathrm{H} + {}^1\mathrm{H} \rightarrow {}^2\mathrm{H} + e^+ + \nu_e$), the reaction rate per g s is

$$r_{ab} = \rho X_a X_b \frac{N_A}{A_a A_b (1 + \delta_{ab})} f(\rho, T)\, g(T). \tag{20.7a}$$

The mean lifetime in seconds for particle a interacting with b is

$$\tau_a = \left[\rho \frac{X_b}{A_b} f(\rho, T)\, g(T) \right]^{-1}. \tag{20.8a}$$

The rate of destruction for particle a by b in numbers per cm^3 s is

$$\left(\frac{dn_a}{dt} \right)_b = -(1 + \delta_{ab}) \rho^2 X_a X_b \frac{N_A}{A_a A_b (1 + \delta_{ab})} f(\rho, T)\, g(T) = -(1 + \delta_{ab}) \rho r_{ab}. \tag{20.9a}$$

The rate of energy generation in erg/(g s) is

$$\begin{aligned} \epsilon_{ab} &= 1.6022 \times 10^{-6}\, Q_{ab} \rho X_a X_b \tfrac{N_A}{A_a A_b (1+\delta_{ab})} f(\rho, T)\, g(T), \\ \epsilon_{ab} &= 1.6022 \times 10^{-6} Q_{ab} r_{ab}. \end{aligned} \tag{20.10a}$$

In these equations $f(\rho, T)$ is the electron screening correction [7–9], $g(T)$ is the temperature dependence of the nuclear reaction rate as discussed and tabulated in [10, 11]. Q_{ab}, the energy in MeV released or absorbed by a interacting with b, is given in [10].

20.2.2 Three-Body Interactions

Here $a + b + c \rightarrow d + e + f$, where f may or may not be present. For example, $3\,{}^4\mathrm{He} \rightarrow {}^{12}\mathrm{C} + \gamma$, can be considered this way even though this reaction is really a resonant reaction involving a pair of two-body reactions.

The reaction rate per g s is

$$r_{abc} = \rho^2 X_a X_b X_c \frac{N_A}{A_a A_b A_c (1 + \delta_{ab} + \delta_{bc} + \delta_{ac} + 2\delta_{abc})} f(\rho, T)\, g(T). \tag{20.7b}$$

The mean lifetime for particle a in seconds interacting with particles b and c is

$$\tau_a = \left[\rho \frac{X_b X_c}{A_b A_c} \frac{(1 + \delta_{ab} + \delta_{ac})}{(1 + \delta_{ab} + \delta_{bc} + \delta_{ac} + 2\delta_{abc})} f(\rho, T)\, g(T) \right]^{-1}. \tag{20.8b}$$

The rate of destruction for particle a by b and c in numbers per cm^3 s is

$$\left(\frac{dn_a}{dt}\right)_{bc} = -(1+\delta_{ab}+\delta_{ac})\rho^2 X_a X_b X_c \frac{N_A\, f(\rho,T)\, g(T)}{A_a A_b A_c (1+\delta_{ab}+\delta_{bc}+\delta_{ac}+2\delta_{abc})}$$
$$= -(1+\delta_{ab}+\delta_{ac})\rho r_{abc}. \tag{20.9b}$$

The rate of energy generation in erg/(g s) is

$$\epsilon_{abc} = 1.6022\times 10^{-6}\, Q_{abc}\rho^2 X_a X_b X_c \frac{N_A\, f(\rho,T)\, g(T)}{A_a A_b A_c (1+\delta_{ab}+\delta_{bc}+\delta_{ac}+2\delta_{abc})}$$
$$= 1.6022\times 10^{-6}\, Q_{abc} r_{abc}. \tag{20.10b}$$

The change in the chemical composition for a given atomic nucleus can be obtained by summing all the production and destruction rates. When nuclear reactions are part of a chain (such as the proton–proton chain) the abundances of different atomic nuclei become interrelated and simplifications become possible when equilibrium is attained.

For a discussion on how nuclear reaction rates are calculated, see [12–14]. For a discussion of the various reactions involved in the hydrogen-, helium-, carbon-, oxygen-, and neon-burning processes, see [15–18].

During post-core helium-burning evolutionary phases, significant nuclear energy can be removed by neutrinos produced by plasma, photoelectron, pair, and bremsstrahlung processes. The rate of energy loss produced by these processes is discussed in [17], [19], and [20].

20.2.3 The Solar Neutrino Problem

Nuclear energy production in the Sun should produce a measurable flux of neutrinos on the Earth primarily due to the following nuclear reactions:

$$^1\mathrm{H} + {}^1\mathrm{H} \longrightarrow {}^2\mathrm{H} + e^+ + \nu_e,$$
$$^7\mathrm{Be} + e^- \longrightarrow {}^7\mathrm{Li} + \nu_e + \gamma,$$
$$^8\mathrm{B} \longrightarrow {}^8\mathrm{Be} + e^+ + \nu_e,$$
$$^1\mathrm{H} + {}^1\mathrm{H} + e^- \longrightarrow {}^2\mathrm{H} + \nu_e.$$

Measurement of this neutrino flux would provide confirmation that the nuclear reactions do take place in the Sun and provide important constraints on theoretical models of the Sun, and to this end there are currently four different solar neutrino detector experiments in operation. Unfortunately, the measured neutrino fluxes are less than those predicted by the best theoretical solar models, and this conflict is the basis of the solar neutrino problem. For a detailed discussion of the experiments and the various approaches to modeling the Sun, see [21] and [22], as well as the review papers of Bahcall [23] and [24]. As discussed in [22] and [24], a possible resolution of the solar neutrino problem could arise if neutrinos have mass and they can undergo oscillations from the electron neutrino state into the muon or tau neutrino states, then the measured flux would be less than expected based only on stable electron neutrinos. Future experiments should be able to test this hypothesis.

20.3 EQUATIONS OF STATE

by W. Dean Pesnell

The equation of state (EOS) joins the microscopic world of quantum mechanics and the macroscopic world of astrophysics [25]. Interactions that govern the world of the atom are averaged to form an

EOS. An EOS is usually presented as a table of pressure and internal energy for many values of ρ and T or as a simple formula for easy computation.

The astrophysical EOS has three major parts: P_N (nuclei), $P_{\rm rad}$ (radiation), and P_e (electrons). Other processes, such as Coulomb interactions and statistical correlations, can modify the EOS. See Table 20.1 for components of the EOS.

Table 20.1. *Components of the equation of state.*[a]

Component	Pressure	Internal energy
Black-body radiation	$aT^4/3$	aT^4/ρ
Nondegenerate nuclei[b]	$(\mathcal{R}/\mu)\rho T$	$3(\mathcal{R}/\mu)\rho T/2$
Nondegenerate electrons	$N_e kT = (\mathcal{R}/\mu_e)\rho T$	$\frac{3}{2}N_e kT = \frac{3}{2}(\mathcal{R}/\mu_e)\rho T$
Degenerate electrons[c,d,e,f]	$Af(x)$	$Ag(x)$
Coulomb corrections[g,h] [1–3]	$-P_N h(U_D)$	$-3P_N h(U_D)/\rho$

Notes

[a] Approximate formulas for optically thin radiation are shown in [4]. Nuclei can crystallize in white dwarfs and the crusts of neutron stars [5].

[b] $\mathcal{R} = 8.3145 \times 10^7$ erg K^{-1} mol^{-1}.

[c] $A = 6.0023 \times 10^{22}$ dyn cm^{-2}.

[d] $f(x) = x(2x^2-3)\sqrt{1+x^2} + 3\ln(x+\sqrt{1+x^2})$.

[e] $g(x) = 8x^3(\sqrt{1+x^2}-1) - f(x)$.

[f] $Bx^3 = \rho/\mu_e$, $B = 9.739 \times 10^5$ mol cm^{-3}.

[g] $U_D = e^2/(R_D kT)$, $R_D^2 = kT/(4\pi e^2 N_e)$, $R_D = 6.90(T/N_e)^{1/2}$ cm.

[h] $h(U_D) = 0.3U_D^{3/2}/(1.03921 + U_D^{1/2})$.

References

1. Koester, D. 1976, *A&A*, **52**, 415
2. Salpeter, E.E., & Zapolsky, H.S. 1967, *Phys. Rev.*, **158**, 876
3. Lai, D., Abrahams, A.M., & Shapiro, S.L. 1991, *ApJ*, **337**, 612
4. Raymond, J.C., Cox, D.P., & Smith, B.W. 1976, *ApJ*, **204**, 290
5. Lamb, D.Q., & Van Horn, H.M. 1975, *ApJ*, **200**, 306

In normal stars the electron contribution to the EOS is the most complicated. Material inside a star is ionized by collisions and radiation. The populations of the electron energy levels are distorted by the close proximity of ionized material. The upper states dissolve and lower energy levels are perturbed from those of an isolated atom. Several ways of approaching this problem are as follows.

Stellingwerf [26, 27] used a simplified atomic model including H, He, and two averaged easily ionized metals. The resulting analytic model is surprisingly accurate and shows that the EOS is insensitive to the upper levels, unlike the opacity.

Eggleton, Faulkner, and Flannery [28] use a fit to the electron degeneracy integrals and force pressure ionization at about the correct density. The EOS uses both tabulated and analytic fits. This EOS is used in Iben's evolution code and in some studies of the Sun.

Mihalas, Däppen, and Hummer [29] use an occupancy probability to smoothly remove the electrons from each state and give a table of values.

Rogers [30] developed a Planck–Larkin partition function that smoothly ionizes the electrons in the usual ionization zone. He also approximates pressure ionization by distorting and removing the electron energy levels as the density of atoms increases.

Both electrons and nuclei can be in a degenerate form. The pressure is greatly enhanced over the nondegenerate value when the repulsive nature of the Fermi–Dirac statistics becomes very large [25]. The electron contribution to the EOS is summarized in Figure 20.1. The degeneracy parameter η has

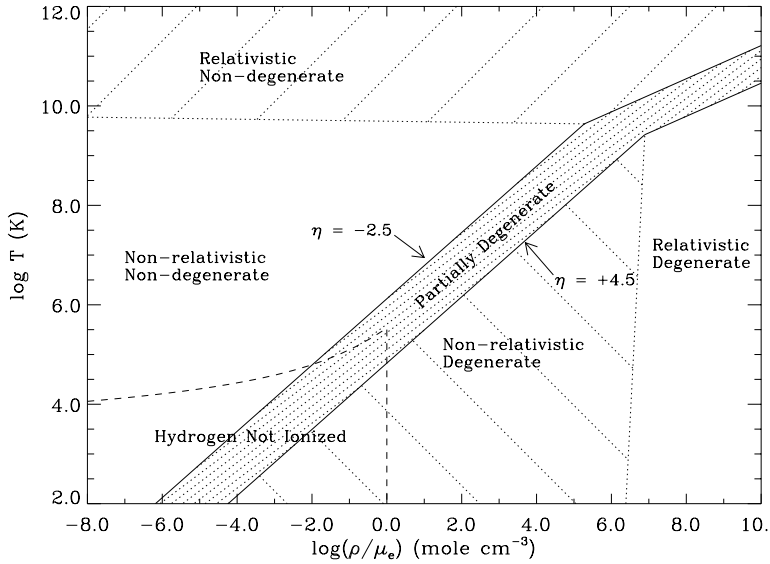

Figure 20.1. The electron contribution to the EOS, defined in the ρ-T plane. Approximate regions of degeneracy, hydrogen ionization, and relativistic effects are shown. The area of partial degeneracy is defined where corrections to P_e in an expansion in η are $< 1\%$. In the nondegenerate, relativistic region ($T > 6 \times 10^9$ K), the effects of e^-–e^+ pairs become important. Adapted from [25].

the limits $-\eta \gg 0$ in nondegenerate matter and $\eta \gg 0$ in degenerate matter.

Degenerate nuclei can never be treated as an ideal gas. Nuclear densities ($\rho \geq 10^{14}\,\mathrm{g\,cm^{-3}}$) imply average separations on the order of a nucleus. The strong nuclear force becomes important and the EOS must incorporate nonideal gas corrections [31].

For $T < 4000$ K, the effect of molecules becomes important. Statistical equilibrium is used to find the concentration of the molecular and atomic components. At extremely low temperatures and high densities (such as in the interior of gas giant planets), the formation of metallic hydrogen is important [32].

Derivatives of EOS variables are an important part of a table or fitting function. Stellar evolution codes require the compressibilities (χ_ρ and χ_T), adiabatic indices (Γ_1, $\Gamma_3 - 1$, and Γ_2), and specific heats (c_V and c_P). As there are two dependent functions of two independent variables (plus composition, see [33]), four derivatives are required to completely specify the EOS and should be tabulated with the dependent variables to increase the numerical accuracy of their interpolation.

20.4 STELLAR OPACITIES

by Arthur N. Cox

The Los Alamos [34–39] and Livermore [40–45] opacities include the bound–bound, bound–free, free–free, and electron scattering processes. Collective effects of the free-electron scattering have been studied definitively by Boercker [46]. Low-temperature opacities including molecular absorptions have been calculated by Los Alamos workers and by Alexander [47, 48], Alexander and Ferguson [49], and by Kurucz [50]. The composition for elements heavier than hydrogen and helium in the solar mixture is given by Grevesse [51–53]. More opacity information is given in Chapter 5.

20.5 ELECTRON CONDUCTION
by Arthur N. Cox

At high densities in stars at advanced evolution stages, sometimes energy can be significantly transported by the flow of electrons. The effective opacity then is reduced to a total opacity κ_T given by the formula

$$1/\kappa_T = 1/\kappa_R + 1/\kappa_C,$$

with κ_R being the purely radiative opacity and κ_C being the conductive opacity that is related to the conductivity ν_C in the relation

$$F = -\nu_C \, dT/dr.$$

The conductive opacity then is

$$\kappa_C = 4acT^3/3\rho\nu_C.$$

The Cox and Tabor [37] tables included this electron conductivity (and a sharp cutoff for the infinite opacity for photons at frequencies below the plasma frequency). With the improvements from the Mestel [54] treatment to those of Hubbard and Lampe [55] and Canuto [56], more recent opacities no longer allowed for this effect in the opacity tables. A simple fit for the conductive opacity is from Sweigart [57]. Fits to the Hubbard and Lampe (nonrelativistic electrons) and Canuto (relativistic electrons) tables are given by Iben [58]. Recent conductivities for neutron star material are given by Itoh et al. [59].

20.6 ELEMENT DIFFUSION
by Arthur N. Cox

The diffusive settling of all elements, except hydrogen, occurs in stars. In very special cases, the absorption of photons and their outward momentum can result in a net outward acceleration for isotopes that are in specific ionization and excitation states. Usually surface convection zones are slightly drained of helium and the Z composition elements, but that effect can be overcome if the depleted outer layers are simultaneously blown away in a stellar wind. Similarly, enhancement of special elements, as seen mostly in Ap, Bp, and Am stars [60], is reduced by stellar winds. Formulations for calculating diffusive settling are given by Burgers [61] and Michaud, Fontaine, and Charland [62], using diffusion coefficients by Paquette et al. [63, 64]. A good review is by Michaud and Vauclair [65].

20.7 MIXING IN STARS
by Arthur N. Cox

A difficult problem in stellar evolution involves the degree of mixing of isotopes that have been segregated by diffusion or are burned at different rates by nuclear reactions. In deep layers where hydrogen is being converted to helium, helium is being burned to carbon and oxygen, or even further nuclear reactions are occurring for more massive stars, any mixing-in of hydrogen or helium will greatly affect this processing and its time scale. The existence of short-lived radioactive isotopes like ^{99}Tc in some stellar atmospheres provides the strongest evidence for mixing. In surface layers, mixing (dredging up) processed material into a surface convection zone can significantly change the observed stellar composition. Very sensitive spectroscopic determinations of some isotopes can probe aspects of stellar evolution, especially in late evolution stages for the red giants and supergiants with deep surface convection zones. Mixing can produce subtle effects, such as moving carbon into hydrogen- and helium-rich material, increasing its opacity, and then causing a superadiabatic gradient that convects

and mixes even more. This gradient of temperature steeper than that given by the adiabatic relations between temperature, density, and pressure cannot exist without convective motions that are very effective in mixing, even in the presence of a magnetic field.

Evidence of transport of angular momentum in the Sun is found in its almost solid body rotation to very deep layers. Its primordial angular momentum is carried somehow to the surface and then magnetically braked. The observation of essentially the primordial beryllium abundance, however, indicates little deep mixing to high-temperature burning layers of solar convection zone material. How angular momentum can be transported without moving matter is a current problem in solar evolution.

Analysis of mixing is complicated. Even a small mass loss can expose compositions that are either depleted or enhanced in some isotopes and confuse conclusions about any diffusive separation or mixing that has occurred.

A good exposition of mixing in general is by Kippenhahn [66].

Some mixing processes are as follows:

- Convection caused by temperature gradients that are superadiabatic [67].
- Overshooting beyond the formal superadiabatic convecting layers [68, 69].
- Semiconvection where mixing occurs just enough to make a subadiabatic gradient [70].
- Merging of isotopes with differing diffusion or radiation levitation rates [71].
- Turbulence resulting from differential rotation shearing layers [72].
- Goldreich–Schubert–Fricke instability in noncylindrically rotating layers [73, 74].
- Meridional (Eddington–Sweet) circulation caused by rotation [5, 75, 76].
- Nonradial pulsations in composition gradient layers (Kato mechanism and Rayleigh–Taylor instability) [77, 78].
- Angular momentum transfer by internal gravity waves [68].
- Diffusion of magnetic fields inside stars [79].

Some effects that impede mixing are as follows:

1. Composition gradients with the normal situation of higher mean molecular weight material being deeper, requiring more superadiabaticity (Ledoux criterion) [25, 80].
2. Magnetic fields that constrain motions across the field lines [81].

20.8 STAR FORMATION

by W. Dean Pesnell

Stars are formed by the collapse of interstellar clouds. Such clouds have $\rho \sim 10^{-20}$ g cm^{-3} and temperatures near 20 K. The gravitational energy released during the collapse either heats the material or is radiated away to space [82]. If the pressure at the center of a spherical cloud of mass $\mathcal{M}$ and radius R exceeds the pressure of an homogeneous sphere,

$$P_c > \frac{G\rho\mathcal{M}}{2R}, \tag{20.11}$$

the cloud cannot collapse. A cloud with $\mathcal{M} = 10\mathcal{M}_\odot$, $R \sim 0.3$ pc, and the density listed above is stable in our Galaxy. Interstellar magnetic fields, rotation, and cloud motion also prevent a cloud from collapsing [83]. In certain cases, magnetic fields can actually carry away angular momentum and promote cloud collapse [84].

Current star formation theories use triggers to overcome the internal pressure and begin the gravitational runaway. Shocks from supernova explosions or density waves can be triggers. Massive stars emit UV radiation, creating ionization shock fronts in the surrounding material, inducing additional collapses.

The biggest hurdle in star formation is rotation. All clouds will rotate, because of the velocity shear in the galaxy if nothing else. As the collapse proceeds, conservation of angular momentum requires the core to spin more quickly. If this is followed to a radius of $1R_\odot$, the star will be rotating faster than the speed of light. The scenario in Table 20.2 is more acceptable.

Table 20.2. *Stages of star formation* [1].

Stage	Feature	Length (yr)
Initial collapse	Disk and central core	10^5
Viscous accretion	Dissipates rotation	10^4–10^5
Cleansing	Strong winds	10^7

Reference

1. Ruden, S.P., & Pollack, J.B. 1991, *ApJ*, **375**, 740

The presence of a disk explains the presence of strong bipolar flows around Herbig–Haro objects [85]. Magnetic fields are examined in [86]. Once contraction has begun, magnetic fields assist the collapse by transporting angular momentum away from the central object.

20.9 PRE-MAIN-SEQUENCE EVOLUTION

by W. Dean Pesnell

Pre-main-sequence evolution follows a protostar to the main sequence. The protostar enters this phase with a high luminosity and large radius. As the star collapses, it moves along the Hayashi track, an almost vertical line in the Hertzsprung–Russell (HR) diagram [87]. When the core becomes radiatively stable, the star turns to the left and, moving along a line of roughly constant radius, contracts in the core until hydrogen burning sets in and the star settles onto the main sequence. Three divisions in mass of the final star are made:

1. Low mass, $\mathcal{M} < 1\mathcal{M}_\odot$ [88–90].
2. Low mass, $1\mathcal{M}_\odot < \mathcal{M} < 8\mathcal{M}_\odot$ [90, 91].
3. High mass, $\mathcal{M} > 8\mathcal{M}_\odot$ [90, 92, 93].

The luminosity in the early stages of evolution comes from an accretion shock at the “surface” of the protostar [94]. Accurate calculations of the evolution require a robust numerical scheme [95] and treatment of deuterium burning [88]. For rotation effects see [96].

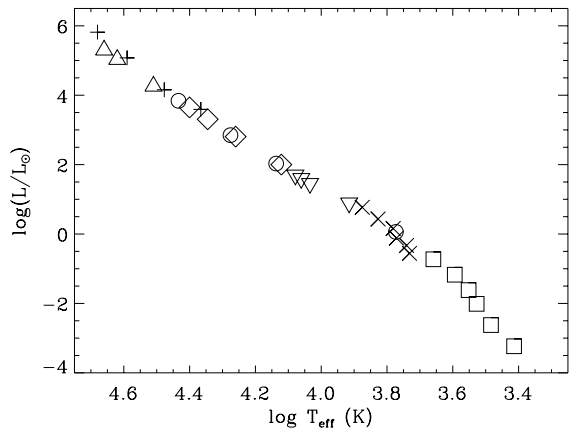

Figure 20.2. A theoretical HR diagram of the zero-age main sequence for Population I stars. The symbols, diamond, triangle, inverted triangle, square, plus sign, circle and × correspond to references [97–103].

20.10 MAIN-SEQUENCE POPULATION I STARS
by W. Dean Pesnell

The main-sequence (MS) is the area of the HR diagram where the greatest density of stars is observed. In the theoretical HR diagram, the MS is the locus of core hydrogen-burning models. Typical surface compositions for Population I stars are $Y = 0.28$ and $Z = 0.02$. Figure 20.2 is an aggregation of theoretical zero-age main-sequence stars (ZAMS) with masses ranging from $0.1\mathcal{M}_\odot$ to $60\mathcal{M}_\odot$. Theoretical luminosity functions are $L \propto \mathcal{M}^{4.5}$ ($\mathcal{M} < 7\mathcal{M}_\odot$) and $L \propto \mathcal{M}^3$ ($M > 7\mathcal{M}_\odot$). The lower limit of the MS is $0.08\mathcal{M}_\odot$, which is not sufficient to begin hydrogen fusion reactions [104]. The upper limit of about $100\mathcal{M}_\odot$ is due to a slowly growing and apparently, not limited in amplitude, pulsational instability driven by the temperature sensitivity of the CNO reaction [105, 106].

Observationally η Car seems to be as massive as $140\mathcal{M}_\odot$ from its place in the Hertzsprung–Russell diagram, but all other stars in our Galaxy and the Magellanic Clouds seem to have less than $100\mathcal{M}_\odot$.

20.11 MAIN-SEQUENCE POPULATION II STARS
by W. Dean Pesnell

Population II stars have a ZAMS slightly below that of Population I stars. Typical surface compositions for Population II stars are $Y = 0.28$ and $Z = 10^{-3}$. Figure 20.3 is an aggregation of theoretical ZAMS models with masses ranging from $0.25\mathcal{M}_\odot$ to $30\mathcal{M}_\odot$. Theoretical luminosity functions are similar to those of Population I stars.

20.12 STELLAR WINDS
by Stephen A. Becker

With the exception of the Sun, the mass-loss rates in Table 20.3 due to stellar winds of main-sequence stars are derived from radio data as described in [109]. For O stars of all luminosity classes, [109] finds the following equation to be accurate to within 50% using common logs:

$$\log(\dot{\mathcal{M}}_*) = 1.69 \log(L_*/L_\odot) - 15.41.$$

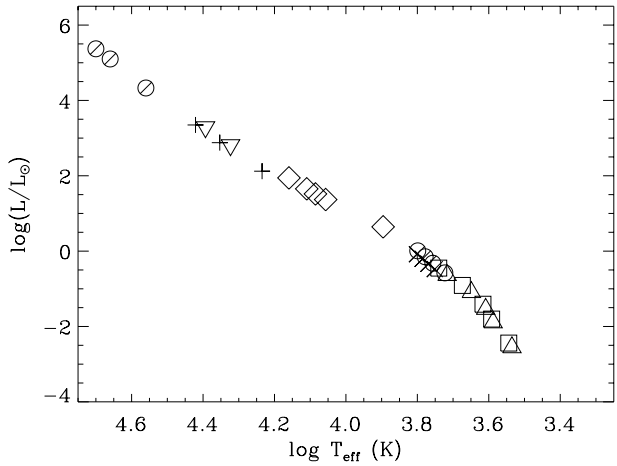

Figure 20.3. A theoretical HR diagram of the zero-age main sequence for Population II stars. The symbols, inverted triangle, circle, diamond, triangle, plus sign, slash in circle, $\times$, and square correspond to references [98, 107, 108, 100, 97, 98, 107, 108].

Here $\dot{\mathcal{M}}_*$ is in $\mathcal{M}_\odot$/yr. For binaries, this relation may not be appropriate.

Table 20.3. *Observed rates of stellar winds.*

Star name	Spectral class	$\log T_{\rm eff}$	$\log L_*/L_\odot$	$\mathcal{M}_*/\mathcal{M}_\odot$	$\log_{10}\mathcal{M}_*$ ($\mathcal{M}_\odot$/yr)	Reference
CygOB2 #7	O3 If	4.65	6.0	82	< 4.9	[1]
HD15570	O4 If+	4.62	6.2	88	-5.0	[1]
HD190429A	O4 If+	4.62	6.1	77	< 4.7	[1]
HD14947	O5 If+	4.61	5.9	64	< -4.8	[1]
CygOB2 #11	O5 If	4.61	6.0	69	< -5.1	[1]
HD15558	O5 III	4.63	6.0	78	< -4.8	[1]
CygOB2 #9	O5 If+	4.61	6.4		-4.9	[1]
HD210839	O6 I(n)fp	4.62	5.9	55	< -5.5	[1]
CygOB2 #5	O6f+O7f	4.60	6.4		-4.5	[1]
HD57060	O7 Iafpvar	4.56	6.3	46	< -5.3	[1]
HD166734	O7.5f+09 I	4.54	5.9		-4.8	[1]
HD151804	O8 Iaf	4.52	6.1	79	-5.0	[1]
HD152408	O8 Iafpe	4.52	6.0	63	-4.7	[1]
HD149757	O9 V	4.53	4.9	24	< -6.8	[1]
HD36486	O9.5 II	4.49	5.7	23	-6.0	[1]
HD37742	O9.7 Ib	4.48	5.8	60	-5.7	[1]
HD37128	B0 Ia	4.42	5.6	32	-5.6	[1]
HD38771	B0.5 Ia	4.36	5.6	32	-6.0	[1]
HD152236	B1 Ia+	4.30	5.9	29	-5.1	[1]
HD169454	B1 Ia+	4.30	6.0	30	-5.4	[1]
κ Cas	B1 Ia+	4.30	5.4	29	-5.6	[2]
P Cyg	B1 Iap	4.09	5.1	17	-4.8	[2]
ρ Leo	B1 Ib	4.31	4.9		-6.2	[2]
HD190603	B1.5 Ia+	4.28	5.7		-5.5	[1]

Table 20.3. *(Continued.)*

Star name	Spectral class	$\log T_{\rm eff}$	$\log L_*/L_\odot$	$\mathcal{M}_*/\mathcal{M}_\odot$	$\log_{10}\mathcal{M}_*$ ($\mathcal{M}_\odot$/yr)	Reference
χ^2 Ori	B2 Ia	4.24	5.5		−5.7	[2]
σ^2 CMa	B3 Ia	4.17	5.1	26	−5.9	[2]
55 Cyg	B3 Ia	4.15	5.1	26	−6.5	[2]
CygOB2 #12	B8 Ia+	4.06	6.1		−4.5	[1]
β Ori	B8 Ia	4.06	5.5		−6.2	[1]
γ Cyg	A2 Ia	3.96	5.3		< -6.8	[1]
Sun	G2 V	3.76	1.0	1.0	−13.6	[3]

References

1. Howarth, I.D., & Prinja, R.K. 1989, *ApJS*, **69**, 527
2. Underhill, A. 1982, in *Stars With and Without Emission Lines*, edited by A. Underhill and V. Doazan (National Technical Information Service, Springfield, VA), NASA Special Publication SP-456 B, p. 140
3. Noci, G. 1988, in *Mass Outflows from Stars and Galactic Nuclei*, edited by L. Branichi and R. Gilmozzi (Kluwer Academic, Dordrecht), p. 11

Wolf–Rayet stars are a class of very luminous, very hot stars whose spectra have broad emission lines of He and may also show broad emission lines of carbon or nitrogen. WR stars appear to be the hydrogen-exhausted interior of stars which have undergone extreme mass loss. The observed mass-loss rates due to stellar winds for a sample of WR stars which are thermal radio emitters is given in Table 20.4 [110]. Typical mass-loss rates for WR stars are greater than those of O stars.

20.13 STELLAR EVOLUTION TRACKS: MASSIVE AND INTERMEDIATE-MASS STARS

by Stephen A. Becker

The evolutionary track that a stellar model traces in an HR diagram is somewhat code dependent. Many stellar evolution codes are currently being used, and they produce different results *in part* due to uncertainties in the input physics (such as the opacity, the equation of state, and the nuclear reaction rates), uncertainties in the modeling of physical phenomenon (such as the treatment of convective overshoot and semiconvection, the handling of nonadiabatic convection, and how non-quasi-static phases of evolution are approximated), different initial conditions (such as the composition, whether nonsolar abundance ratios are considered in the heavy-element mixture, and mass loss), and modeling techniques. Consequently, stellar evolution tracks in the literature change with time as the input physics improves and modeling approaches change. The state of the art is such that the results of different codes may differ in detail, but the codes do agree on the general qualitative features of the evolutionary tracks. To reflect the diversity of approaches a representative sample of stellar evolution tracks of massive and intermediate-mass stars with the same Population I composition is presented for comparison in Figures 20.4, 20.5, and 20.6. This presentation is by no means all-inclusive, as a search of the literature would reveal.

Table 20.4. *Wolf–Rayet mass loss rates.*

Name (HD)	Spectral class	$\log_{10} \dot{\mathcal{M}}_*$ ($\mathcal{M}_\odot$/yr)
190918	WN4.5+O9.5 IB	−4.52
50896	WN5	−4.12
193077	WN5+OB	−4.73
193576	WN5+O6	−4.62
191765	WN6	−4.13
192163	WN6	−4.02
151932	WN7	−4.31
214419	WN7+O	< -4.61
165763	WC5	−4.50
156385	WC7	<4.46
152270	WC7+O5–8	−3.98
192641	WC7+O5	−4.48
193793	WC7+O4–5	−4.10
192103	WC8	−4.36
68273	WC8+O9 I	−4.09
168206	WC8+O8–9 IV	≤ -4.38
164270	WC9	≤ -4.54

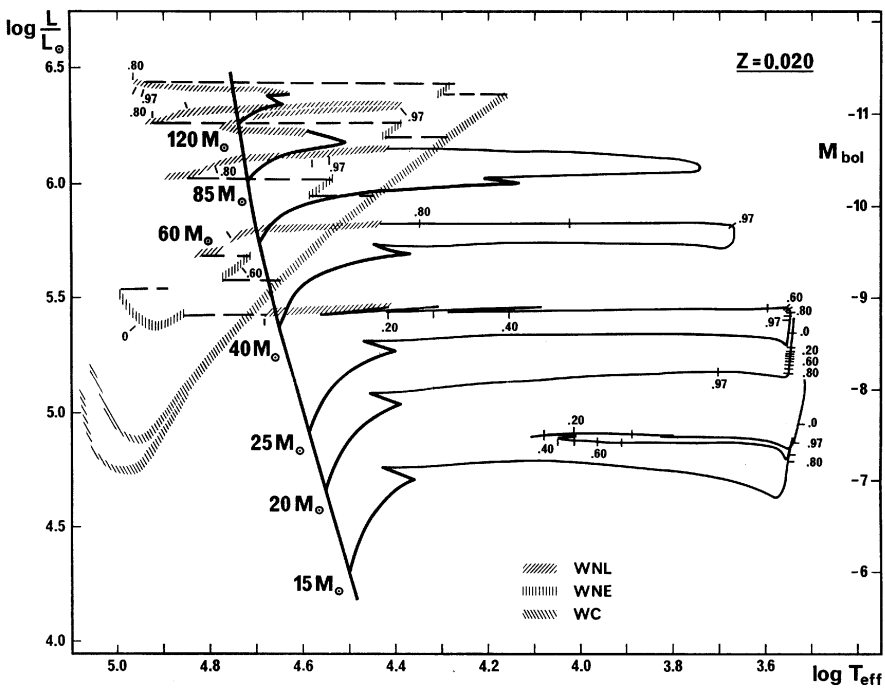

Figure 20.4. Theoretical HR diagram showing evolutionary tracks running from the ZAMS stage to the end of central carbon burning for stellar models of initial mass in the range (15–120)$\mathcal{M}_\odot$ and initial composition $(X, Y, Z) = (0.70, 0.28, 0.02)$. Evolution is followed with mass loss and includes the effect of moderate overshooting during the different convective core phases [111].

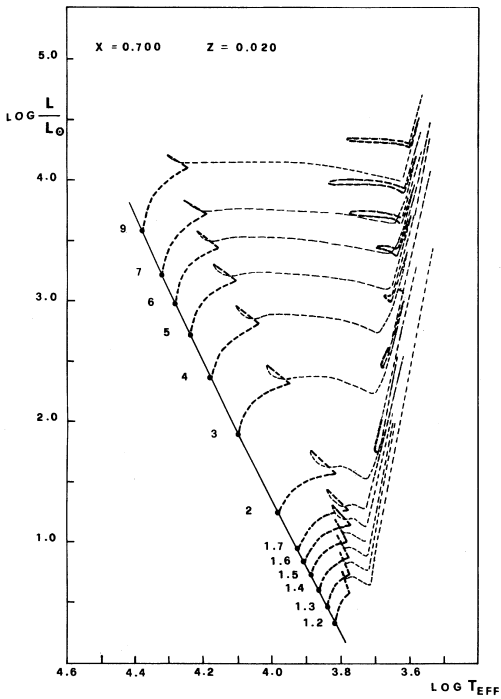

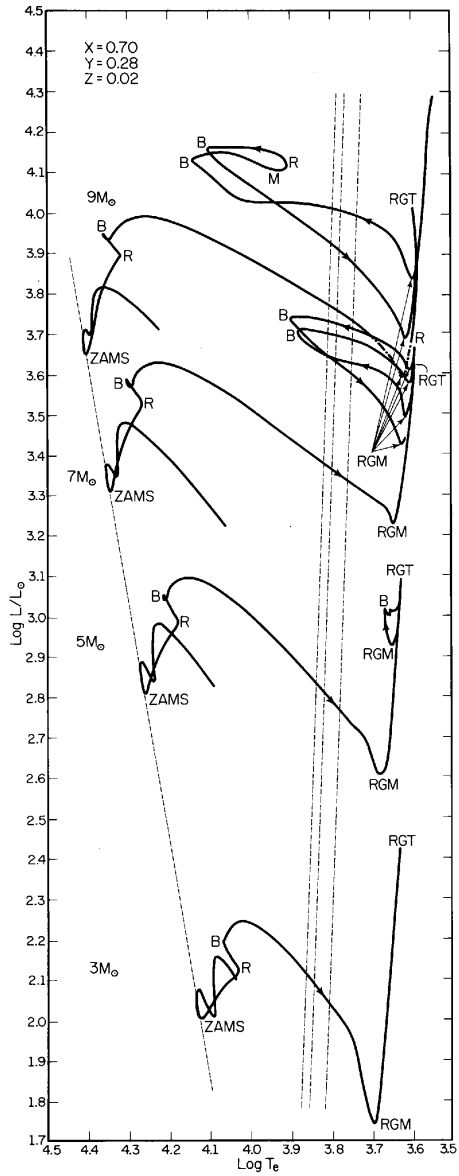

Figure 20.5. (Left) Theoretical HR diagram showing evolutionary tracks running from the ZAMS stage to the start of the thermally pulsing AGB or core carbon ignition for stellar models of initial mass in the range (1.2–9)$\mathcal{M}_\odot$ and initial composition $(X, Y, Z) = (0.70, 0.28, 0.02)$. Evolution is followed without mass loss but with convective overshoot ($d/H_P = 1$) present during the hydrogen and helium burning convective core phases [112].

.

Figure 20.6. (Right) Theoretical HR diagram showing evolutionary tracks running from the ZAMS stage to the start of the thermally pulsing AGB or core carbon ignition for stellar models of initial mass in the range (3–9)$\mathcal{M}_\odot$ and initial composition $(X, Y, Z) = (0.70, 0.28, 0.02)$. Evolution is followed without mass loss or convective overshoot [97].

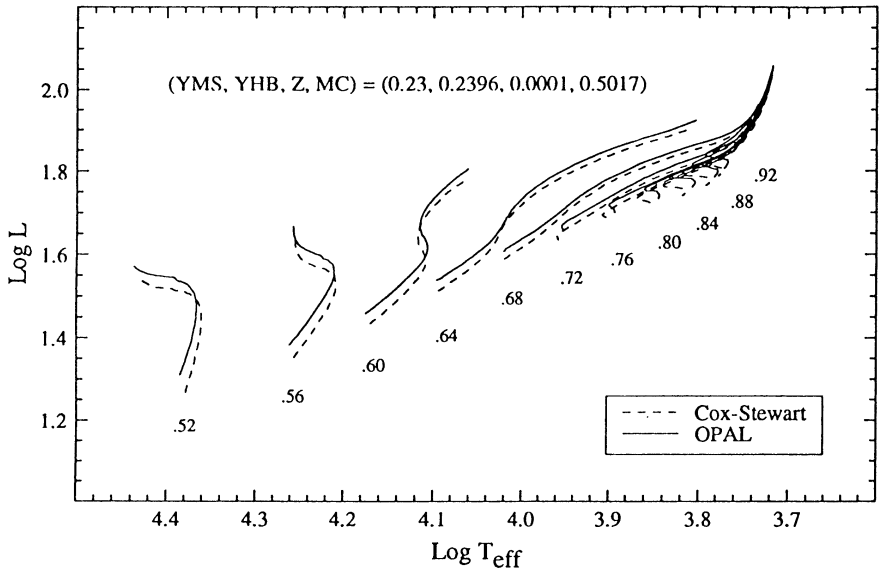

Figure 20.7. Horizontal branch evolution for Population II stars using both the Los Alamos and Livermore opacities. The stellar parameters are the main-sequence helium mass fraction, the increased dredged-up helium content on the zero-age horizontal branch, the heavy-element mass fraction, and the helium core mass (in solar units).

20.14 EVOLUTION TO RED GIANT BRANCH

by W. Dean Pesnell

The evolution of stars with mass less than $3.5\mathcal{M}_\odot$ creates a long-lived evolutionary stage called the asymptotic giant branch (AGB) [113, 114]. The stars either burn helium quiescently or as flashes in a degenerate core. The resulting evolution paths lie very close to the Hayashi track the star followed during its initial collapse. See [99, 108].

20.15 HORIZONTAL BRANCH EVOLUTION

by Arthur N. Cox

Population II stars lose of the order of $(0.1–0.2)\mathcal{M}_\odot$ as red giants in the HR diagram only after igniting helium at their centers and then quickly evolve to the horizontal branch. Details of how this mass loss occurs at the core helium flash and the tracks they follow have not been clearly presented. It is known that the core flash does not occur at the stellar center, and the multidimensional hydrodynamics that occur are complicated. The zero-age horizontal branch extends blueward of the main sequence for the lowest ($\sim 0.5\mathcal{M}_\odot$) masses, and these lowest-mass stars can move directly into the white dwarf region as their helium cores burn to carbon and oxygen. With significant surface hydrogen, the stars evolve redward to the AGB, but for very thin layers the stars are already white dwarfs. Horizontal branch tracks using both the Los Alamos and Livermore opacities are given by Yi, Lee, and Demarque [115] in Figure 20.7. The evolution of the central temperature and density in these models is given in Figure 20.8.

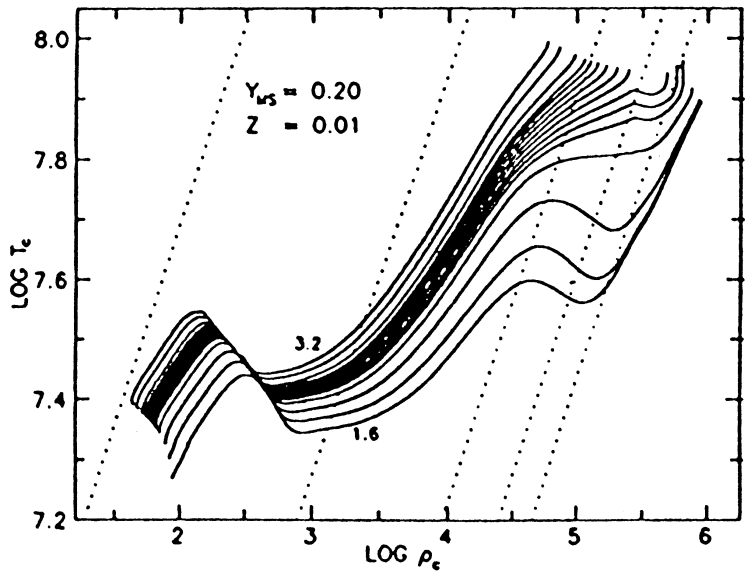

Figure 20.8. Evolutionary dependence of the central temperature (T_C) and density (ρ_C) for the models between 1.6 and 3.2$\mathcal{M}_\odot$. The dotted lines are lines of constant degeneracy parameter at the center of the model, $\eta_C = -4$, 0.5, 10, and 15 from left to right. Adapted from [99, 108].

20.16 RED GIANT MASS-LOSS RATES

by Stephen A. Becker

Based on a study of normal red giant and supergiant stars, Reimers [116, 117] has proposed the following semiempirical scaling law for stellar mass loss:

$$\dot{\mathcal{M}}_* = 4 \times 10^{-13} \eta (L_*/L_\odot) \left(\frac{g_*}{g_\odot} \frac{R_*}{R_\odot} \right)^{-1} . \tag{20.12}$$

Here $\dot{\mathcal{M}}_*$ is in units of $\mathcal{M}_\odot$/yr, g is the gravitational acceleration at the stellar surface, and η is a dimensionless factor introduced to take into account the uncertainty in the mass-loss rate determination or behavioral differences between different types of stars. Typically, η is considered to be in the range of 1/3 to 3. Reimers [117] states that his relation should not be applied to stars of distinctly different properties like OH-IR stars [where the rate appears to be an order of magnitude larger than given by Equation (20.12)], F stars, and C stars. The accuracy of this relation can be tested by comparing with the observed mass-loss rates given in Table 20.5. Care should be taken in this comparison because while $\mathcal{M}_*$ and L_* are inferred from observation, the values for R_* and $\mathcal{M}_*$ are generally not, and consequently, the values listed are estimates which can vary considerably from author to author. For $\eta = 1$ the Reimers mass-loss rate agrees with the observed mass loss given in Table 20.5 to within a factor of 3 for most of the stars listed (although there are some cases where it is a factor of 10 off). Examples of mass-loss rates determined for OH-IR stars and C stars are given in Tables 20.6 and 20.7. Other mass-loss studies and formulations have been done (for representative examples, see [118–120]).

Table 20.5. *Measured mass-loss rates for normal giant and supergiant stars and the Sun.*

Star	Spectral type	T_e	$R_*/R_\odot$	$\log L_*/L_\odot$	$\mathcal{M}_*/\mathcal{M}_\odot$	$\dot{\mathcal{M}}_*$ ($\mathcal{M}_\odot$/yr)	Reference
HR 8752	G0 Ia	5000	1000	5.5	30	1×10^{-5}	[1]
α Ori	M2 Iab	3900	860	5.0	10	4×10^{-6}	[2]
α Sco	M1.5ab	3540	625	4.68	~ 18	1×10^{-6}	[3]
χ Her	M6 III	2670	810	4.56	3.1	7.2×10^{-7}	[2]
$\delta^2$2 Lyr	M4 II	3490	420	4.32	2.8	4.8×10^{-8}	[2]
g Her	MG III	3250	630	4.28	4.0	1.3×10^{-7}	[2]
α HerA	M5 II	3200	460	4.23	7.6	8.2×10^{-8}	[2]
L^2 Pup	M5 IIIe	2825	600	3.92	2.6	4.8×10^{-8}	[2]
31 Cyg	K4 Ib	3800	202	3.91	6.2	4×10^{-8}	[4]
32 Cyg	K5 Iab	3800	188	3.82	8	2.8×10^{-8}	[4]
W Hya	M5 IIIe	2825	510	3.77	1.5	1.1×10^{-7}	[2]
R Dor	M8 Ie	2230	680	3.73	1.5	3.9×10^{-7}	[2]
R Lyr	M5 III	3394	210	3.57	2.2	1.4×10^{-8}	[2]
δ Sge	M2 II	3600	140	3.43	8	2×10^{-8}	[5]
ζ Aur	K4 Ib	3950	140	3.41	8.3	6×10^{-9}	[4]
ρ Per	M4 II–III	3500	150	3.36	5.0	1.2×10^{-8}	[2]
β Peg	M2 II–III	3600	110	3.23	1.7	1.1×10^{-9}	[2]
22 Vul	G3 Ib–II	5200	> 40	2.99	4.3	6×10^{-9}	[6]
α Boo	K1 IIIp	4250	27	2.23	1.1	2×10^{-10}	[2]
Sun	G2 V	5780	1	1	1	2.6×10^{-14}	[7]

References

1. Lambert, D.L., & Luck, R.E. 1978, *MNRAS*, **184**, 405
2. Judge, P.G., & Stencel, R.E. 1991, *ApJ*, **371**, 357
3. Hagen, H-J., Hempe, K., & Reimers, D. 1987, *A&A*, **184**, 256
4. Che, A., Hempe, K., & Reimers, D. 1983, *A&A*, **126**, 225
5. Reimers, D., & Schröder, K-P. 1983, *A&A*, **123**, 241
6. Reimers, D., & Che-Bohenstenzel, A. 1986, *A&A*, **166**, 252
7. Noci, G. 1988, in *Mass Outflows from Stars and Galactic Nuclei*, edited by L. Branichi and R. Gilmozzi (Kluwer Academic, Dordrecht), p. 11

Table 20.6. *Observed mass-loss rates for OH-IR stars.*

Star	$\dot{\mathcal{M}}_*$ ($\mathcal{M}_\odot$/yr)	Reference
PZ Cas	1.1×10^{-5}	[1]
Z Cas	2.3×10^{-7}	[1]
RS Vir	6.8×10^{-7}	[1]
OH 11.5+0.1	3.2×10^{-6}	[1]
OH 12.8−1.9	1.6×10^{-5}	[1]
OH 13.1+5.0	8.7×10^{-5}	[1]
OH 16.1−0.3	1.1×10^{-6}	[1]
OH 18.3+0.4	1.6×10^{-4}	[1]
OH 18.5+1.4	3.3×10^{-6}	[1]
OH 18.8+0.3	1.1×10^{-6}	[1]
OH 20.2−0.1	1.4×10^{-5}	[1]
OH 20.7+0.1	1.3×10^{-4}	[1]
OH 21.3+0.5	2.6×10^{-4}	[1]
OH 25.1−0.3	3.1×10^{-6}	[1]
OH 26.2−0.6	3.8×10^{-7}	[1]
OH 26.5+0.0	1.2×10^{-4}	[1]
OH 30.1−0.7	3.1×10^{-5}	[1]
OH 30.1−0.2	4.0×10^{-6}	[1]

Table 20.6. *(Continued.)*

Star	$\dot{\mathcal{M}}_*$ ($\mathcal{M}_\odot$/yr)	Reference
OH 30.7−10.4	1.1×10^{-4}	[1]
OH 31.0−0.2	1.6×10^{-5}	[1]
OH 31.0+0.0	6.1×10^{-6}	[1]
OH 32.0−0.5	8.9×10^{-5}	[1]
OH 32.8−0.3	2.4×10^{-4}	[1]
OH 35.6−0.3	3.4×10^{-5}	[1]
OH 36.9+1.3	4.7×10^{-7}	[1]
OH 39.7+1.5	9.7×10^{-7}	[1]
OH 39.9−0.0	7.7×10^{-6}	[1]
OH 44.8−2.3	4.0×10^{-5}	[1]
OH 45.5+0.1	1.8×10^{-5}	[1]
OH 53.6−0.2	2.0×10^{-6}	[1]
OH 75.3−1.8	1.6×10^{-4}	[1]
OH 83.4−0.9	4.6×10^{-6}	[1]
OH 104.9+2.4	3.5×10^{-5}	[1]
OH 127.8−0.0	9.4×10^{-5}	[1]
OH 127.9−0.0	1.4×10^{-4}	[1]
OH 138.0+7.2	2.2×10^{-5}	[1]
OH 138.0+7.3	5.3×10^{-6}	[1]
OH 141.7+3.5	1.1×10^{-5}	[1]
OH 231.8+4.2	1.3×10^{-4}	[2]

References

1. Netzer, N., & Knapp, G.R. 1987, *ApJ*, **323**, 734
2. Knapp, G.R., & Morris, M. 1985, *ApJ*, **292**, 640

Table 20.7. *Mass loss rates for selected carbon stars.*

Star	Type	$\dot{\mathcal{M}}_*$ ($\mathcal{M}_\odot$/yr)	Reference
CIT 6	C4,3	2.3×10^{-6}	[1]
RY Dra	C4,4	5.1×10^{-6}	[2]
TU Gem	C4,6	9.0×10^{-7}	[2]
UU Aur	C5,3	3.0×10^{-7}	[1]
X Cnc	C5,4	2.5×10^{-7}	[2]
Y Hya	C5,4	3.9×10^{-7}	[2]
Y CVn	C5,4	1.0×10^{-7}	[3]
TX Psc	C6,2	1.6×10^{-7}	[1]
R Scl	C6,II	4.2×10^{-6}	[1]
V Hya	C6,3e	4.0×10^{-6}	[3]
V460Cyg	C6,3	4.0×10^{-7}	[2]
VY UMa	C6,3	1.5×10^{-7}	[2]
U Cam	C6,4e	1.08×10^{-5}	[2]
ST Cam	C6,4	2.2×10^{-7}	[2]
RV Cyg	C6,4	7.4×10^{-7}	[2]
RY Mon	C6,5	8.5×10^{-7}	[2]
T Lyr	C6,5	6.0×10^{-7}	[2]
TW Hor	C7,2	8.0×10^{-8}	[1]
NP Pup	C7,2	1.3×10^{-7}	[1]
U Hya	C7,3	4.9×10^{-7}	[1]
UX Dra	C7,3	7.5×10^{-8}	[2]
T Ind	C7,3	8.0×10^{-8}	[1]
Z Psc	C7,3	9.1×10^{-8}	[2]
IRC+20370	C7,3e	1.0×10^{-5}	[3]

Table 20.7. *(Continued.)*

Star	Type	$\dot{\mathcal{M}}_*$ ($\mathcal{M}_\odot$/yr)	Reference
V Cyg	C7,4e	1.04×10^{-5}	[2]
IRC+40540	C8,3,5	1.4×10^{-5}	[1]
T Dra	C8e	1.3×10^{-6}	[3]
IRC+10216	C9,5	5.5×10^{-5}	[1, 3]
IRC+00499	Ne	4.4×10^{-6}	[3]
IRC+50096	N	6.3×10^{-6}	[3]
R Lep	N6e	2.1×10^{-6}	[3]
CRL 482	C	1.7×10^{-5}	[3]
CRL 865	C	2.3×10^{-5}	[3]
IRC−10236	C	4.7×10^{-6}	[3]
IRC+20326	C	2.3×10^{-5}	[3]
CRL 2155	C	1.7×10^{-5}	[3]
CRL 2199	C	1.3×10^{-5}	[3]
IRC+40485	C	2.6×10^{-6}	[3]
CRL 3068	C	7.3×10^{-6}	[3]
CRL 3099	C	1.5×10^{-6}	[3]
RU Vir	R3ep	9.5×10^{-6}	[3]

References

1. Judge, P.G., & Stencel, R.E., 1991, *ApJ*, **371**, 357
2. Wannier, P.G., Shai, R., Anderson, B.G., & Johnson, H.R. 1990, *ApJ*, **358**, 251
3. Knapp, G.R., & Morris, M. 1985, *ApJ*, **292**, 640

20.17 ASYMPTOTIC GIANT BRANCH EVOLUTION

by Stephen A. Becker

The evolutionary behavior of a low-mass star on the asymptotic giant branch (AGB) in the HR diagram is illustrated in Figure 20.9 from [113]. Such stars are the major source of planetary nebulae and they evolve into white dwarfs. A detailed description of the AGB phase of evolution for stars of low and intermediate mass can also be found in [113]. A more recent review of the evolutionary phase can be found in [121, 122].

20.18 WHITE DWARFS AND NEUTRON STARS

by Arthur N. Cox and Stephen A. Becker

After a star has become a red giant, it can have blue loops in the HR diagram as both Population I and II stars exhibit, it can have no loops, or it can evolve directly to the blue. Thus white dwarfs can be formed either directly from the Population II red giant tip or from the results of heavy mass loss from Population I or II stars after the AGB evolution. After a superwind ejects essentially all surface hydrogen, stars evolve across the top of the HR diagram at about $10^4 L_\odot$ with a rapidly decreasing surface radius. These are the (DO) pre-white dwarfs, the helium (DB) white dwarfs, and the hydrogen (DA) white dwarfs. Neutron stars (or even black holes) are the result of a supernova explosion when the core of the highly evolved star collapses to create an explosion of the outer stellar layers. See Chapter 16 for a list of pulsars that are these neutron stars seen in all photon energy bands as they rotate, exposing photon sources.

A review of the masses and evolutionary states of white dwarfs can be found in [123]. The evolution and cooling of white dwarfs is discussed in [124] and [125]. The equilibrium mass-radius

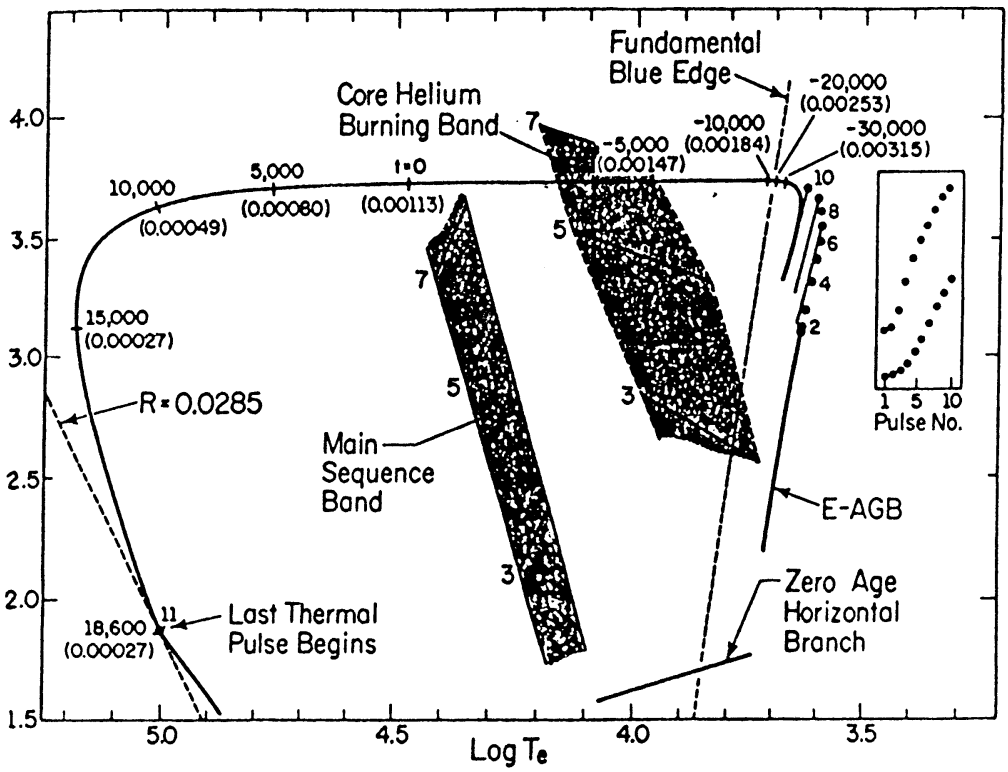

Figure 20.9. Evolutionary track in the HR diagram of an AGB model of mass $0.6\mathcal{M}_\odot$, initial composition $(Y, Z) = (0.25, 0.001)$. After burning helium in its core on the horizontal branch, the model arrives at the early-AGB track to burn helium in a shell; the hydrogen-burning shell is extinguished. The early-AGB phase is terminated when hydrogen reignites and thermal pulsing begins. The location of the model at the start of each pulse is indicated by heavy dots. Excursions in the HR diagram during the extended postflash dip and recovery period are shown for pulses 7, 9, and 10. Dots in the panel in the extreme right-hand portion of the diagram describe the excursion in luminosity during extended dips for all pulses that occur on the AGB track. Evolution time ($t = 0$ when $T_e = 30\,000$ K) and mass in the hydrogen-rich envelope (in parentheses) are shown at various points along the track leaving the AGB phase after the tenth pulse. Time is in years, and $\mathcal{M}_e$ and R are in solar units. A line of constant radius passes through the location of the beginning of the eleventh pulse when the model has become a hot white dwarf. The dashed line is a blue edge for pulsation in the fundamental mode for a model of mass $0.6\mathcal{M}_\odot$ and $(Y, Z) = (0.25, 0.001)$. Shown for orientation purposes are the rough evolutionary tracks, during core hydrogen- and core helium-burning phases for $(Y, Z) = (0.28, 0.001)$ and masses 3, 5, and $7\mathcal{M}_\odot$.

relation for zero-temperature white dwarfs is reviewed in [126]. A general review of the theoretical and observational aspects concerning white dwarfs can be found in [127–129].

20.19 BINARY STAR EVOLUTION

by Stephen A. Becker

The previous sections of this chapter have dealt with the evolutionary behavior of single stars. Considerations of binary star evolution opens an area of investigation which is much more complicated and cannot be adequately summarized in the limited space available here. Reference [130] provides a brief introduction to the subject of binary star evolution, while [122, 131] provide excellent general reviews of this subject.

20.20 THEORY VERSUS OBSERVATION IN THE HR DIAGRAM

by Stephen A. Becker

As noted in Section 20.13, there are various uncertainties in stellar evolution calculations, particularly those associated with convection, and the best approach to constrain these (when better data or better theory is lacking) is through comparison with observational data. The HR diagram provides a useful method of comparison, especially when applied to star clusters and certain types of variable stars. Representative examples of what can be learned from such comparisons are given in [132–136].

REFERENCES

1. Clayton, D.D. 1968, *Principles of Stellar Evolution and Nucleosynthesis* (McGraw-Hill, New York), p. 436
2. Cox, J.P., & Giuli, R.T. 1968, *Principles of Stellar Structure*, Vol. 2, *Application to Stars* (Gordon and Breach, New York), p. 644
3. Collins, G.W. 1989, *The Fundamentals of Stellar Astrophysics* (Freeman, New York), p. 100
4. Kippenhahn, R., & Weigert, A. 1990, *Stellar Structure and Evolution* (Springer-Verlag, Berlin), p. 64
5. Tassoul, J.-L. 1978, *Theory of Rotating Stars* (Princeton University Press, Princeton, NJ)
6. Hansen, C.J., & Kawaler, S.J. 1994, *Stellar Interiors* (Springer-Verlag, New York), p. 330
7. Lang, K.R. 1980, *Astrophysical Formulae* (Springer-Verlag, Berlin), p. 385
8. Cox, J.P., & Giuli, R.T. 1968, *Principles of Stellar Structure*, Vol. 1, *Physical Principles* (Gordon and Breach, New York), p. 467
9. Clayton, D.D. 1968, *Principles of Stellar Evolution and Nucleosynthesis* (McGraw-Hill, New York), p. 357
10. Caughlan, G.R., & Fowler, W.A. 1988, *Atomic Data Nucl. Data Tables*, **40**, 283
11. Fowler, W.A., Caughlan, G.R., & Zimmerman, B.A. 1975, *ARA&A*, **13**, 69
12. Lang, K.R. 1980, *Astrophysical Formulae* (Springer-Verlag, Berlin), p. 375
13. Cox, J.P., & Giuli, R.T. 1968, *Principles of Stellar Structure*, Vol. 1, *Physical Principles* (Gordon and Breach, New York), p. 429
14. Clayton, D.D. 1968, *Principles of Stellar Evolution and Nucleosynthesis* (McGraw-Hill, New York), p. 288
15. Lang, K.R. 1980, *Astrophysical Formulae* (Springer-Verlag, Berlin), p. 419
16. Cox, J.P., & Giuli, R.T. 1968, *Principles of Stellar Structure*, Vol. 1, *Physical Principles* (Gordon and Breach, New York), p. 475
17. Kippenhahn, R., & Weigert A. 1990, Stellar *Structure and Evolution* (Springer-Verlag, Berlin), p. 161
18. Clayton, D.D. 1968, *Principles of Stellar Evolution and Nucleosynthesis* (McGraw-Hill, New York), p. 369
19. Cox, J.P., & Giuli, R.T. 1968, *Principles of Stellar Structure*, Vol. 1, *Physical Principles* (Gordon and Breach, New York), p. 512
20. Meyer-Hofmeister, E. 1982, in *Landolt-Börnstein Numerical Data and Functional Relationships in Science and Technology*, Group VI, Vol. 2b (Springer-Verlag, New York), p. 187
21. Cox, A.N., Livingston, W.C., & Matthews, M.S., editors, 1991, *Solar Interior and Atmosphere* (University of Arizona, Tucson)
22. Balantekin, A.B., & Bahcall, J.N., editors, 1995, *Solar Modeling* (World Scientific, Singapore)
23. Bahcall, J.N. 1989, *Neutrino Astrophysics* (Cambridge University Press, Cambridge)
24. Bahcall, J.N. 1996, *ApJ*, **467**, 475
25. Cox, J.P., & Giuli, R.T. 1968, *Principles of Stellar Structure* (Gordon and Breach, New York), Chapters 9 & 24
26. Stellingwerf, R.E., 1975, *ApJ*, **195**, 441
27. Stellingwerf, R.E., 1975, *ApJ*, **199**, 705
28. Eggleton, P.P., Faulkner, J., & Flannery, B.P. 1973, *AAp*, **23**, 325
29. Mihalas, D., Däppen, W., & Hummer, D.G. 1988, *ApJ*, **331**, 815
30. Rogers, F. 1986, *ApJ*, **310**, 723
31. Shapiro, S.L., & Teukolsky, S.A. 1983, *Black Holes, White Dwarfs, and Neutron Stars: The Physics of Compact Objects* (Wiley-Interscience, New York), Sec. 8
32. Hubbard, W.B. 1990, in *The New Solar System*, edited by J.K. Beatty, C.C. Petersen, and A. Chaikin (Sky Publishing, New York), p. 131
33. Pesnell, W.D. 1986, *ApJ*, **301**, 204
34. Cox, A.N., & Stewart, J.N. 1969, Sci. Info. Astr. Council USSR Acad. Sci. Vol. 15
35. Cox, A.N., & Stewart, J.N. 1970, *ApJS*, **19**, 243
36. Cox, A.N., & Stewart, J.N. 1970, *ApJS*, **19**, 612
37. Cox, A.N., & Tabor, J.E. 1976, *ApJS*, **31**, 271
38. Huebner, W.F., Merts, A.L., Magee, N.H., & Argo, M.F. 1977, LA 6760M, Los Alamos Publication
39. Weiss, A., Keady, J.J., & Magee, N.H. 1990, *Atomic Data Nucl. Data*, **45**, 209
40. Iglesias, C.A. & Rogers, F.J. 1991, *ApJ*, **371**, 408
41. Iglesias, C.A. & Rogers, F.J. 1991, *ApJS*, **371**, L73
42. Iglesias, C.A. & Rogers, F.J. 1992, *ApJS*, **79**, 507
43. Iglesias, C.A., Rogers, F.J., & Wilson, B.G. 1992, *ApJ*, **397**, 717
44. Rogers, F.J. & Iglesias, C.A. 1992, *ApJ*, **401**, 361
45. Iglesias, C.A. & Rogers, F.J. 1996, *ApJ*, **464**, 943
46. Boercker, D.B. 1987, *ApJ*, **316**, L95

47. Alexander, D.R. 1975, *ApJS*, **29**, 363
48. Alexander, D.R., Johnson, H.R., & Rypma, R.L. 1983, *ApJ*, **272**, 773
49. Alexander, D.R. & Ferguson, J.W. 1994, *ApJ*, **437**, 879
50. Kurucz, R.L. *IAU Symposium* 149, 225 (see Chapter 5)
51. Grevesse, N. 1991, *A&A*, **242**, 488
52. Grevesse, N. 1991, *A&A*, **232**, 225
53. Grevesse, N. 1991, private communication
54. Mestel L. 1950, *Proc. Cambridge Philos. Soc.*, **46**, 331
55. Hubbard, W.B., & Lampe, M. 1969, *ApJS*, **18**, 279
56. Canuto, V. 1970, *ApJ*, **159**, 641
57. Sweigart, A.V. 1973, *A&A*, **24**, 459
58. Iben, I. Jr. 1975, *ApJ*, **196**, 525; erratum 1993, *ApJ*, **415**, 767
59. Itoh, N., Kohyama, Y., Mastumoto, N., & Seki, M. 1984, *ApJ*, **285**, 758
60. Wolff, S.C. 1983, *The A Stars; Problems and Perspectives*, NASA Special Publication No. 463
61. Burgers, J.M. 1969, *Flow Equations for Composite Gases* (Academic Press, New York)
62. Michaud, G., Fontaine, G., & Charland, Y. 1984, *ApJ*, **280**, 787
63. Paquette, C., Pelletier, C., Fontaine, G., & Michaud, G. 1986, *ApJS*, **61**, 177
64. Paquette, C., Pelletier, C., Fontaine, G., & Michaud, G. 1986, *ApJS*, **61**, 197
65. Michaud, G., & Vauclair, S. 1991, in *Solar Interior and Atmosphere*, edited by A.N. Cox, W.C. Livingston, and M.S. Matthews (University of Arizona Press, Tucson)
66. Kippenhahn, R. 1974, *Late Stages of Stellar Evolution*, IAU Symposium 66 (Reidel, Dordrecht), p. 20
67. Vitense, E. 1953, *Z. Astrophys.*, **32**, 135
68. Schatzman, E. 1991, in *Solar Interior and Atmosphere*, edited by A.N. Cox, W.C. Livingston, and M.S. Matthews (University of Arizona Press, Tucson)
69. Chan, K.L., Nordlund, A., Steffen, M., & Stein, R.F. 1991, in *Solar Interior and Atmosphere*, edited by A.N. Cox, W.C. Livingston, and M.S. Matthews (University of Arizona Press, Tucson)
70. Schwarzschild, M., & Härm, R. 1958, *ApJ*, **128**, 348
71. Vauclair, S., & Vauclair, G. 1982, *ARA&A*, **20**, 37
72. Zahn, J.P. 1983, in *Astrophysical Processes in Upper Main Sequence Stars*, edited by A.N. Cox, S. Vauclair, and J.P. Zahn (Geneva Observatory, Geneva)
73. Goldreich, P., & Schubert, G. 1967, *ApJ*, **150**, 571
74. Fricke, K.J. 1968, *Z. Astrophys.*, **68**, 316
75. Eddington, A.S. 1925, *Observatory*, **48**, 73
76. Sweet, P.A. 1950, *MNRAS*, **110**, 548
77. Kato, S. 1966, *PASJ*, **18**, 374
78. Dilke, F.W.W., & Gough, D.O. 1972, *Nature*, **240**, 262
79. Parker, E.N. 1984, *ApJ*, **281**, 839
80. Ledoux, P. 1947, *ApJ*, **105**, 305
81. Chapman, S., & Cowling, T.G. 1970, in *The Mathematical Theory of Non-Uniform Gases* (Cambridge University Press, Cambridge)
82. Jeans, J.H. 1902, *Philos. Trans. R. Soc. London* A, **199**, 1
83. Spitzer, L. 1968, *Diffuse Matter in Space* (InterScience, New York), Sec. 6
84. Mouschiovios, T.C. 1991, in *Physics of Star Formation*, edited by C.J. Lada and N.D. Kylafis (Kluwer Academic, Dordrecht)
85. Shu, F.H., Adams, F.C., & Lizano, S. 1987, *ARA&A*, **25**, 23
86. Pudritz, R.E., & Carlberg, R.G. 1989, in *Low Mass Star Formation and Pre–Main Sequence Objects* (ESO, Garching), p. 33
87. Hayashi, C. 1966, *ARA&A*, **4**, 171
88. Stahler, S.W. 1988, *PASP*, **100**, 1474
89. Stahler, S.W. 1989, *ApJ*, **347**, 950
90. Iben, I., Jr. 1965, *ApJ*, **141**, 993
91. Palla, F., & Stahler, S.W. 1991, *ApJ*, **375**, 288
92. Lequeux, J. 1985, in *Birth and Infancy of Stars*, edited by R. Luces, A. Omont, and R. Stora (North-Holland, Amsterdam), p. 3
93. Downes, D. 1989, in *Star Forming Regions*, edited by M. Peimbert and J. Jugaku (Reidel, Dordrecht), p. 93
94. Larson, R.B. 1968, *MNRAS*, **145**, 271
95. Winkler, K.-H., & Newman, M.J. 1980, *ApJ*, **236**, 201
96. Pinsonneault, M.H., Kawaler, S.D., Sofia, S., & Demarque, P. 1989, *ApJ*, **338**, 424
97. Becker, S.A. 1981, *ApJS*, **45**, 475
98. Brunish, W.M., & Truran, J.W. 1982, *ApJS*, **49**, 447
99. Sweigart, A.V., Greggio, L., & Renzini, A. 1989, *ApJS*, **69**, 911
100. VandenBerg, D.A., Hartwick, F.D.A., Dawson, P., & Alexander, D.R. 1983, *ApJ*, **266**, 747
101. Maeder, A. 1981, *A&A*, **102**, 401
102. Pesnell, W.D., unpublished
103. Green, E.M., Demarque, P. & King. C.R. 1987, *The Revised Yale Isochrones and Luminosity Functions* (Yale University Observatory: New Haven, CT)
104. D'Atona, F., & Mazzitelli, I. 1985, *ApJ*, **296**, 502
105. Ziebarth, K. 1970, *ApJ*, **162**, 947
106. Stothers, R. 1992, *ApJ*, **392**, 706
107. Iben, I., Jr., & Rood, R.T. 1970, *ApJ*, **159**, 605
108. Sweigart, A.V., Greggio, L., & Renzini, A. 1990, *ApJ*, **364**, 527
109. Howarth, I.D., & Prinja, R.K. 1989, *ApJS*, **69**, 527
110. Prinja, R.K., Barlow, M.J., & Howarth, I.D. 1990, *ApJ*, **361**, 607
111. Maeder, A. 1990, *A&AS*, **84**, 139
112. Bertelli, G., Bressan, A., Chiosi, D., & Angerer, K. 1986, *A&AS*, **66**, 191
113. Iben, I., Jr., & Renzini, A. 1983, *ARA&A*, **21**, 271
114. Sweigart, A.V., & Gross, P.G. 1978, *ApJS*, **36**, 405
115. Yi, S., Lee, Y-W., & Demarque, P. 1993, *ApJ*, **411**, L25
116. Reimers, D. 1975, in *Problems in Stellar Atmospheres and Envelopes*, edited by B. Baschek, W.H. Kegel, and G. Traving (Springer-Verlag, New York), p. 229
117. Reimers, D. 1988, in *Mass Outflows from Stars and Galactic Nuclei*, edited by L. Bianchi and R. Gilmozzi (Kluwer Academic, Dordrecht), p. 25
118. Garmany, C.D., & Conti, P.S. 1984, *ApJ*, **284**, 705
119. Chiosi, C., & Maeder, A. 1986, *ARA&A*, **24**, 239
120. de Jager, C., Nieuwenhuijzen, H., & van der Hucht, K.A. 1988, *A&AS*, **72**, 259

121. Lattanzio, J.C. 1989, in *Evolution of Peculiar Red Giant Stars*, edited by H.R. Johnson and B. Zuckerman (Cambridge University Press, Cambridge), p. 161
122. Iben, I., Jr. 1991, *ApJS*, **76**, 55
123. Weidemann, Y. 1990, *ARA&A*, **28**, 103
124. Iben, I., Jr., & Tutukov, A.V. 1984, *ApJ*, **282**, 615
125. D'Antona, F., & Mazzitelli, L. 1990, *ARA&A*, **28**, 139
126. Hamada, J., & Salpeter, E. 1961, *ApJ*, **134**, 683
127. Cox, J.P., & Giuli, R.T. 1968, *Principles of Stellar Structure*, Vol. 2, *Application to Stars* (Gordon and Breach, New York), p. 874
128. Kippenhahn, R., & Weigert, A. 1990, *Stellar Structure and Evolution* (Springer-Verlag, New York), p. 366
129. Hansen, C.J., & Kawaler, S.D. 1994, *Stellar Interiors* (Springer-Verlag, New York), p. 338
130. Hansen, C.J., & Kawaler, S.D. 1994, *Stellar Interiors* (Springer-Verlag, New York), p. 72
131. Trimble, V. 1983, *Nature*, **303**, 137
132. Maeder, A., & Renzini, A., editors, 1984, *Observational Tests of the Stellar Evolution Theory*, IAU Symposium 105 (Reidel, Dordrecht)
133. Madore, B.F., editor. 1985, *Cepheids: Theory and Observation*, IAU Colloqium 82 (Cambridge University Press, New York)
134. Renzini, A., & Fusi Pecci, F. 1988, *ARA&A*, **26**, 199
135. Chiosi, C., Bertelli, G., & Bressan, A. 1992, *ARA&A*, **30**, 235
136. Bedding, T.R., Booth, A.J., & Davis, J., editors, 1997, *Fundamental Stellar Properties: The Interations Between Observation and Theory*, IAU Symposium 189 (Kluwer Academic, Dordrecht)